Optically transparent self-reinforced poly(ethylene terephthalate) composites: molecular orientation and mechanical properties

P. Rojanapitayakorn[a], P.T. Mather[a,b,*], A.J. Goldberg[c], R.A. Weiss[a,b]

[a]Polymer Science Program, Storrs, University of Connecticut, CT 06269, USA
[b]Department of Chemical Engineering, University of Connecticut, Storrs, CT 06269, USA
[c]Center for Biomaterials, University of Connecticut Health Center, Farmington, CT 06030, USA

Abstract

Self-reinforced composites have been fabricated by compaction of oriented polyethylene terephthalate (PET) fibers under pressure at temperatures near, but below, their melting point. The originally white fiber bundles, which were about 40% crystalline, show increased crystallinity (55%) but optical translucency after processing. Differential scanning calorimetry (DSC) and wide-angle X-ray diffraction (WAXD) were used to study the crystallization and orientation of the fibers, revealing that the degree of crystallinity was somewhat insensitive to compaction conditions while the melting point increased substantially with increasing compaction temperature. Crystalline orientation, gauged using the Hermans orientation parameter from WAXD data, indicated that no significant loss in orientation of the crystalline fraction occurs due to compaction. Mechanical characterization revealed a stepwise decrease in flexural modulus (9.4–8.1 GPa) and concomitant increase in transverse modulus and strength on increasing the compaction temperature from 255 to 259 °C. This transition in behavior was accompanied by a loss of optical transparency and a change in the distribution of amorphous fraction from fine intrafibrillar domains to coarse interfibrillar domains as seen with electron microscopy. We argue then that the mechanical properties of PET compactions are influenced more by orientation of the amorphous phase than that of the crystalline phase. The impact properties of compacted materials, characterized using an unnotched Charpy test method, showed remarkable impact resistance after compaction, with impact toughness decreasing as compaction temperature was increased.
© 2004 Elsevier Ltd. All rights reserved.

1. Introduction

Conventional processing techniques for continuous fiber-reinforced polymers include resin transfer molding and autoclave lamination of fiber-resin prepregs. Common reinforcing fibers include glass, graphite, poly(phenylene terephthalamide) (Kevlar™) and poly(p-phenylene-2,6-benzobisoxazole) (Zylon™). Matrix materials range from thermoplastics to thermosets, the latter employing such polymeric precursors as epoxies, acrylates, urethanes, and bismaleimides as the most common choices, depending on application requirements, especially upper use temperature. The ultimate properties of continuous fiber composites depend strongly on the adhesion between the composite's fiber and matrix as a strong bond is necessary for stress transfer from the matrix to the fiber, allowing the stronger fibers to carry the bulk of the load. Thus, significant effort has been devoted to improving the understanding and technology of fiber–matrix bonding.

A different approach for achieving high modulus/high strength materials from thermoplastic fibers alone is hot compaction, a process in which highly oriented fibers are welded together with minimal sacrifice in the pristine fiber properties [1–22]. Such a process naturally produces a strong fiber–matrix interface, since the two resultant 'phases' are of identical chemistry. Specifically, the composite matrix results from partial melting of the fibers,

---

* Corresponding author. Address: Macromolecular Science and Engineering, Case Western Reserve University, 2100 Adelbert Road, 44106 Cleveland, USA. Tel.: +1 216 368 5861; fax: +1 425 732 7953.
E-mail address: patrick.mather@case.edu (P.T. Mather).

while the reinforcement is derived from the core regions of the original fibers. Hot compaction, or welding, of thermoplastic polymeric fibers near the melting range of the polymer can allow significant retention of the longitudinal mechanical properties of the original fibers, while producing solid objects with good mechanical properties even for loading directions away from the longitudinal fiber axis [1–5]. This technique has drawn the attention of several research groups and has been applied to both amorphous and semi-crystalline polymeric materials.

In particular, Ward and coworkers pioneered the hot compaction technique with fibers prepared from polyethylene [1,2,6–9], polyethylene terephthalate [3,13], polypropylene [4,10–12] and liquid crystalline copolyesters [5,6]. Cohen et al. [16–18] prepared composites from UHMW polyethylene fibers using this idea, finding that by applying a high compaction pressure, coupled with a gradually increasing temperature up to the melting point, a high-performance composite can result. Similarly, Xu and Farris [22] expanded the applicability of PE hot-compaction (termed 'matrix-free composite') to include complex shapes with attractive properties for military applications. Stellbrink et al. [19] also studied the processing technique as applied to a liquid crystalline copolyester with the interesting result that the compacted LCP fibers exhibited high impact energy absorption, although the influence of compaction conditions on impact resistance was not clarified. Wright and coworkers [20,21] used hot compaction to prepare composites from poly(methyl methacrylate), PMMA, for biomedical applications, revealing substantial improvements in flexural, tensile, fracture toughness, and fatigue properties of compacted PMMA specimens compared to the virgin materials.

While both amorphous and semicrystalline polymers have been studied for hot compaction processing, the semicrystalline polymers are more attractive due to their intrinsically higher mechanical properties in original fiber form and the ability of the melted material to recrystallize after heating and compression. The present report focuses on a study of hot compaction applied to PET, a thermoplastic widely used for the manufacturing of cloth, containers, and films. Oriented PET fibers may have high modulus (up to 30 GPa) and strength (1 GPa), and as such, they have a potential to be compacted into high performance composites. Although the hot compaction of PET has been previously described [3], the morphology of the fiber and the interphase region is complicated and questions remain with regard to secondary crystallization and orientation of the melted fibers in the heat treatment process. The attractive mechanical properties reported in that prior work inspired us to study PET hot compaction in further detail.

Several recent studies [23–27] have reported differences in crystallization between unoriented and oriented PET, findings expected to affect the polymer orientation and physical properties of compacted PET. In the present study,

a simplified method based on previous reports [3,16,19] was used to prepare compacted PET. We note that a wide range of processing protocols have been adopted for hot compaction studies, when applied to similar or identical materials. For example, Ward and coworkers [1–5,15] used a 2-step pressure sequence at constant processing temperature, while Cohen and coworkers [16–18] control the melting temperature by using changes in the hydrostatic pressure. We also note that in a very recent paper that appeared after review of the present paper, Hine and Ward described a one-step compaction process [14]. In contrast, Stellbrink et al. [19] began by making thin sheets of compacted fibers at constant pressure and temperature, followed by compaction of such stacked sheets at a temperature slightly higher than the melting point of the fiber.

For simplicity, we adopted a 'one-step method' that follows the protocol of Stellbrink et al. [19] but without the successive compaction step. Such a method was expected to yield thick and strong composites with a one-step process and optimized time-profiles of pressure and temperature. Differential scanning calorimetry (DSC) and wide-angle X-ray diffraction (WAXD) were used to quantitatively examine plaques resulting from hot compaction of PET fibers. The melting behavior and orientation of compacted materials were studied at different compaction temperatures, and the influence of process conditions on flexural modulus, flexural strength, and impact toughness was determined. Finally, the internal microstructure of the compacted materials was examined by electron microscopy employing an etching technique that extracted only the amorphous polymer fraction. Such imaging revealed surprising sensitivity of the distribution of amorphous phases within the materials and consequently the optical clarity and mechanical properties.

2. Experimental

2.1. Materials

A commercial yarn of PET (R&M International Sales Corp. USA) having a linear density of about 1500 denier (1 denier (de) = 9 g/km) and tenacity of 8 g/de, according to the manufacturer, was used in this study. The molecular weight of 53,000 g/mol was estimated from intrinsic viscosity measurements in *o*-chlorophenol at $T = 25\,°C$ [26]. Each yarn contained about 136 filaments per fiber tow, with the filaments having an average diameter of 33 μm. The density of the filaments was about 1.37 g/cm^3 and the axial shrinkage of the unloaded filaments upon melting was 13%. The modulus and strength of the yarn measured in tension with a crosshead speed of 1 mm/min and gauge length of 200 mm were 10 GPa and 800 MPa, respectively.

2.2. Hot compaction processing

A bundle of PET fibers was wound around a square, open metal frame, with an opening of 50×50 mm^2, using a custom-built reciprocating winding machine that allowed for the control of winding speed and tension. A schematic diagram of the process and photographs of the original and wound fibers are shown in Fig. 1. A linear spinning rate of 40 cm/min and a tension of approximately 6 N were used for all of the experiments. Specimen thickness was controlled by the number of layers of wound fibers. The wound specimen was then sandwiched between two 45 mm $\times$ 45 mm metal plates and compacted in a hydraulic press (Wabash Metal Product, Inc., Model 50-1212-2TM) with platens heated to a prescribed temperature between 245 and 270 °C that covered and exceeded the melting range of the PET fibers. The temperature of the samples being compacted was monitored by a thermocouple mounted at the mold surface.

It was suggested in previous studies [1–6] that a two-step pressurization be used at the compaction temperature, T_{com}; i.e. light pressure ~ 1.85 MPa followed by the application of a higher pressure of 32.4 MPa and cooling under pressure and during recrystallization. However, our preliminary studies showed that use of a single pressurization with a pressure intermediate between the pressures suggested above by Rasburn et al. [3] can successfully produce well-compacted materials, as evidenced by a combination of optical transparency with high molecular orientation and crystallinity. The single-step hot compaction method used is shown in Fig. 1. The wound-fiber mold was inserted into the preheated press and compressed with a pressure within the range $20 < P < 60$ MPa soon after the temperature of the fibers reached the desired temperature. The pressure was applied for 15 to 30 min. The pressure best suited for the single-step process was first determined using a compaction temperature of $T_{com} = 259$ °C and by examination of the clarity and integrity of the compacted plaques and the orientation of the fibers that was retained. Once the pressure to be used was identified, the influence of compaction times of 15 and 30 min. was investigated. All assemblies were cooled under pressure at a cooling rate of approximately 20 °C/min to $T = 100$ °C, at which point any recrystallization was completed according to DSC measurements. Finally, the specimens were removed from the press and allowed to cool to room temperature under ambient conditions. 'Isotropic' specimens, confirmed as such by the absence of orientation in WAXD patterns, were obtained by reheating a previously compacted sample to 270 °C, which was above the melting point, and annealing under light pressure (~ 8 MPa) for 30 min. Shorter times were insufficient to completely relax the orientation of the original fibers, and substantially longer times resulted in sample discoloration. The discoloration was probably a result of degradation of the PET during compaction, which was recently discussed by Hine and Ward [13]. This is a concern that was raised after the present study was completed. However, neither the thermal, nor the mechanical property data that are presented indicate that polymer degradation was a significant factor in these experiments, though clearly some caution is advisable with respect to the results discussed here and the possibility of effects of
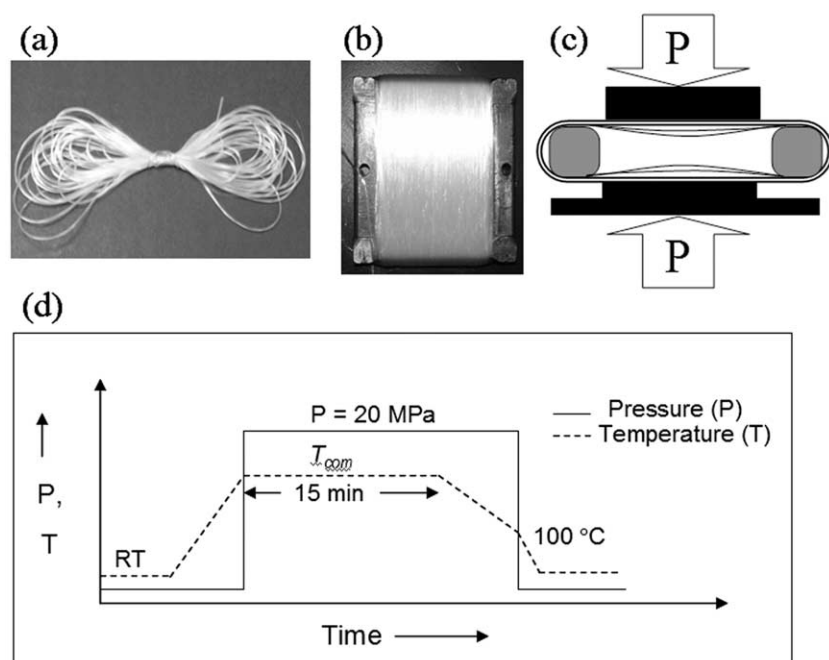

Fig. 1. Processing scheme for hot compaction processing: (a) commercial PET fiber yarn, (b) fiber wound on open square frame, (c) compaction of wound fibers, (d) schematic processing profile.

polymer degradation similar to those experienced by Hine and Ward [13].

2.3. Characterization

Thermal analysis was carried out with a Perkin Elmer DSC-7 differential scanning calorimeter using a scanning rate of 20 °C/min. The degree of crystallinity (Φ_D) for each specimen was obtained from the melting enthalpy, ΔH_m, using the relation:

$$\Phi_D = \Delta H_m / \Delta H^{\circ}_m \times 100\% \tag{1}$$

where ΔH°_m is the enthalpy of fusion for 100% crystalline PET, 135 J/g. [27] The melting point (T_m) was taken as the temperature corresponding to the peak in the melting endotherm. Representative sections were obtained from compacted specimens by simple microtoming with a razor.

The microstructure of hot-compacted samples was characterized by wide-angle X-ray diffraction (WAXD) and small angle X-ray scattering (SAXS). The WAXD measurements were conducted in transmission mode using Cr Kα radiation ($\lambda = 0.2291$ nm), a Bruker AXS 2D position-sensitive detector, and a sample-to detector distance of 6.0 cm. Cu Kα radiation ($\lambda = 0.1541$ nm) was employed for SAXS experiments with a sample to detector distance of 64.5 cm. Specimens of 1 mm thickness were cut from plaques of compacted materials using a razor blade with collection times of 30 min providing adequate signal-to-noise in the patterns collected. The data were corrected for background scattering and a PIN-diode beam stop was used to determine the required correction for air scattering.

An Instron universal testing machine, Model 1011, was used to measure the tensile and flexural properties of both the original fibers and compacted materials. Following previous reports [3] a gauge length of 200 mm and crosshead speed of 1 mm/min were used. Because of the high stiffness and strength of the compacted specimens, a flexural geometry was used for mechanical property measurements to avoid clamping difficulties. The flexural modulus and strength of the compacted specimens were measured using a three-point bending test in accordance with ASTM standard D790. A crosshead speed of 1 mm/min, a bridge span (L) of 24 mm, and a specimen width (W) of 10 mm were used. A sample thickness (D) of 1.5 mm was chosen, yielding an L/D ratio of 16. Anisotropic samples obtained from compaction were cut using a diamond saw in either the longitudinal or the transverse direction with respect to the original fiber alignment direction. Some compacted materials cut along the longitudinal direction did not break or yield within the 5% strain limit dictated by ASTM D-790 for determining a yield strength. Therefore, to facilitate comparisons between the different compacted samples, the flexural stress at 5% strain was used to describe the higher strain mechanical properties of the plaques cut in the longitudinal direction; this stress is hereafter termed '5% flexural strength.'

Charpy impact tests were carried out on unnotched specimens with a Ceast pendulum impact tester (model DAS-2000WIN) using a sample support span of 5 cm, a vertical impacting rod with radius 5 mm and an impact energy of 15 J. The unnotched specimen is more suitable for fiber-reinforced composite materials, where an artificial crack, i.e., the notch, can mask the effect of the embedded fiber orientation (see ASTM Standard D4812). The compacted plaques were cut along the fiber direction into $3 \times 10 \times 65$ mm^3 specimens, which were loaded into the instrument support with the 3×65 mm^3 edge exposed for impact. None of the samples compacted below the melting point of the original fibers broke in the impact test. Instead, a local fracture occurred at the point of impact, leading to excessive bending of the bar and a pulling out of the sample from the holder vise. The dissipated energy determined from the impact experiment therefore only represents that absorbed by the local fracture. Transient flexural load data in all cases revealed a maximum in the force–time trace, but with more or less dissipated energy, depending on the compaction conditions. Thus, to adequately represent the impact characteristics, both the transient force data and cumulative energy absorbed were recorded for each impact test. The unnotched impact resistance, I_s (J/m), was calculated from Eq. (2),

$$I_s = E/w \tag{2}$$

where E is the cumulative energy and w is the width of the specimen. The values reported are averages based on measurements of at least 10 specimens.

Cross-sections of the compacted samples, cut either parallel or normal to the fiber orientation with a razor blade, were examined by scanning electron microscopy (SEM) using a Philips ESEM 2020. The specimens were etched for 24 h in n-propylamine to selectively remove amorphous material, following the procedure of Chu and Wilkes [28]. The etched samples were then coated with Pd/Au and examined using the SEM operated at 20 kV and a magnification of 500.

3. Results and discussion

Pressure and pressure history are key factors in the compaction process, since pressure can control the shrinkage of the fibers and promote densification. For an arbitrary compaction time of 15 min, the microstructure (degree of compaction and orientation) was sensitive to the applied pressure for $20 < P < 40$ MPa, as evidenced by variation of the fiber orientation measured by WAXD. Increasing pressure during the compaction process at constant temperature was expected to increase orientation due to an increased PET melting point and crystallinity [29].

However, the open sides of the sample fixture allowed plastic flow of the amorphous polymer fraction at high-applied pressures, which reduced the uniaxial molecular orientation. That effect was only noticeable for $P > 60$ MPa, so for the studies reported herein, the compaction pressure was fixed at 20 MPa while the processing temperature was varied.

Compaction times, t_{com} (see Fig. 1) less than 15 min were insufficient to complete the fiber compaction process, as was evidenced by the opacity of the compacted specimens. Compaction times of 15 to 30 min produced acceptable samples as judged by the physical appearance of the sample and from the WAXD and DSC data as described in the discussion below. Varying the time within that interval had a negligible effect on the products, a finding consistent with the report by Stellbrink et al. [19], who observed that varying the compaction time between 5 and 60 min for a liquid crystalline polymer with low crystallinity did not affect the mechanical properties and appearance of the compacted materials. On the basis of these observations, a fixed compaction time of 15 min was used for all the samples reported in the present study.

Wound PET fibers were compacted at various temperatures between 249 and 261 °C. Within this range of processing temperatures, the initially white, opaque fiber bundles were transformed into transparent or translucent plaques. At higher processing temperatures ($T_{com} > 262$ °C), the fibers completely melted, resulting in opaque, unoriented plaques upon recrystallization. Fig. 2(a) shows that a compacted fiber plaque prepared at 255 °C was relatively transparent; however, the plaques became more opaque as the processing temperature increased, as shown in Fig. 2(b) and (c). The plaque processed at 259 °C, Fig. 2(b), was still translucent, but for the material processed above the melting point of the PET fibers, the plaque was white and opaque, Fig. 2(c).

The melting behavior of the compacted materials as measured by DSC is shown in Fig. 3. For samples melted incompletely, i.e. other than trace (vi), there was a significant effect of the compaction temperature on the melting point, and although the shapes of the melting endotherms changed, there was relatively little effect on the degree of crystallinity, Φ_D, for compaction temperatures between 249 and 261 °C, see Fig. 4 and Table 1. The melting point of the fibers compacted at 249 °C was higher than that of the original fiber, and the melting point
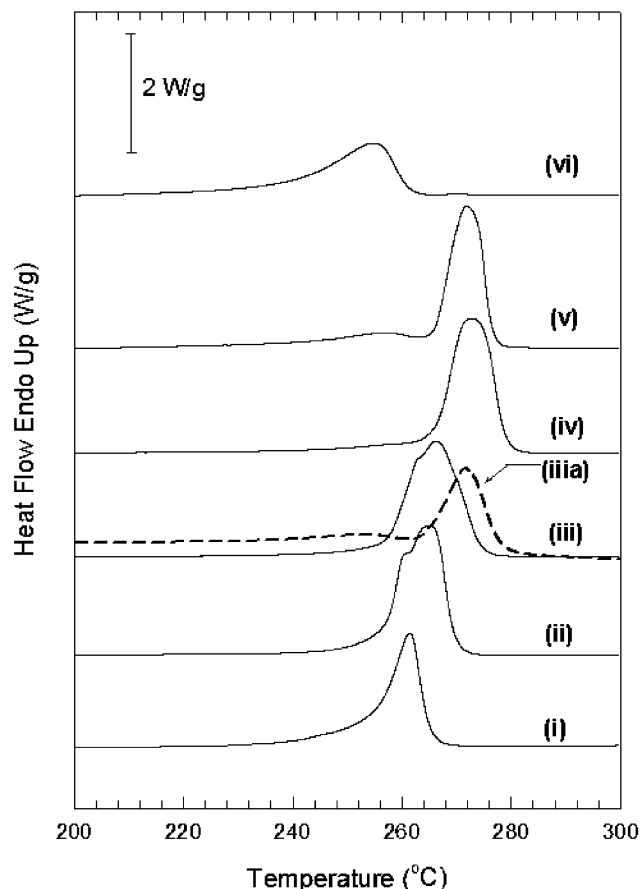

Fig. 3. DSC heating thermograms of: (i) original PET fiber, PET composites compacted at (ii) 249 °C, (iii), 255 °C, (iv) 259 °C, and (v) 261 °C, and (vi) 264 °C. All curves are from the first heating scan of as received fibers or compacted fibers. Note that (iiia) curve represents the thermogram of fibers after being annealed at 255 °C for 15 min and cooled to 25 °C at 30 °C/min.

increased as the compaction temperature was increased to the melting point of the original fibers, 262 °C. For compaction temperatures above the melting point of the fibers, there was a large decrease in both T_m and the degree of crystallinity, see Fig. 4 and Table 1. These results agree well with those reported by Rasburn et al. for PET fiber compaction [3,29].

To discern the separate effects of compaction pressure and annealing temperature, we examined the melting behavior of the original fibers that were annealed at 255 °C at ambient pressure in the DSC. The resulting DSC heating trace is shown as trace iii(a) of Fig. 3. In
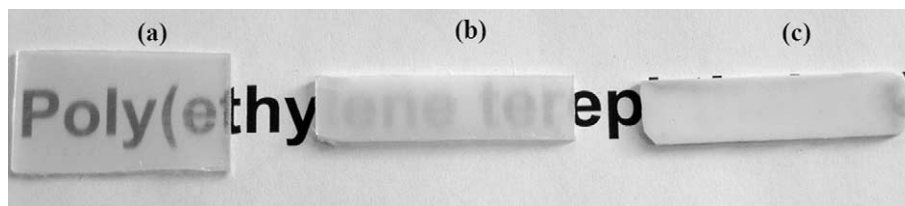

Fig. 2. Photographs of PET plaques prepared at different compaction temperatures, T_{com}: (a) 255 °C, (b) 259 °C and (c) 270 °C. The compacted plaques are each about 1.5–2 mm thick.
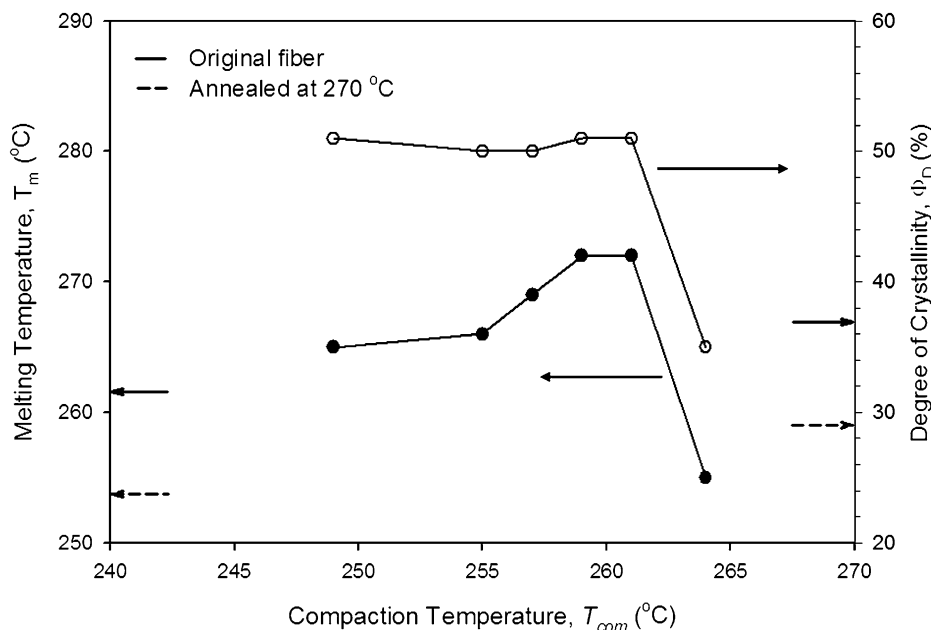
Fig. 4. Melting temperature (●) and degree of crystallinity (○) for PET fiber compactions as a function of the compaction temperatures. Dashed arrows denote the melting temperature and degree of crystallinity for unoriented PET (annealed at 270 °C), while solid arrows denote the melting point and degree of crystallinity for an original unconstrained PET fiber.

comparison to the original fibers, the melting point and degree of crystallinity increased, although the crystallinity of the annealed fibers was still less than for fibers compacted at the same temperature. Moreover, the DSC trace for 255 °C annealing of unconstrained fibers was quite similar in shape to that for compaction at a higher 261 °C, though with a significantly lower crystallinity. Thus, both pressure and temperature during annealing play an important role in dictating the subsequent melting behavior of the materials.

While the melting point of the compacted fibers increased with increasing compaction temperature below the melting point of the original fibers, the melting endotherm of the compacted samples became broader than that for the original fibers. In addition, for annealing temperatures below 259 °C, the endotherm exhibited a peak or shoulder on the lower temperature side of the major peak, the temperature of which corresponded closely to the melting temperature of the original fibers. Curiously, the compacted sample with the broadest melting endotherm,

compacted at 255 °C (see trace (iii) in Fig. 3) was also the clearest sample (see Fig. 2(a)). Above a compaction temperature of 255 °C, the melting point exhibited a more rapid increase with increasing compaction temperature (see Figs. 3 and 4) and the samples became more opaque in appearance. Those observations suggest that above an optimum compaction temperature, a significantly higher fraction of the fiber melts and recrystallizes under pressure—the result being a higher temperature crystal, but with more scattering of the sample, presumably due to the larger crystallite size, less orientation of the recrystallized polymer or scattering from an interphase region of recrystallized polymer surrounding the remnants of the original oriented fibers.

When the compaction temperature was increased to just below the melting point of the original fibers, a second, lower temperature endotherm appeared in the DSC thermogram, trace (v) in Fig. 3, with a peak temperature close to that of the completely melted and recrystallized sample,

Table 1
Result of the calculation of degree of crystallinity from DSC and WAXD, orientation parameter

Compaction temperature (°C)	Φ_D from DSC (%)	Φ_x from WAXD (%)	$\langle\cos^2\phi\rangle$	f_2
Fiber	37	44	0.65	0.48
249	51	57	0.62	0.43
255	50	54	0.64	0.46
257	50	56	0.65	0.48
259	51	55	0.65	0.48
261	51	54	0.62	0.43
264	35	38	0.37	0.06
270	29	31	0.35	0.03

trace (vi). We suggest that this lower temperature endotherm in the sample compacted close to the fiber melting point, in this case 1 °C below the melting point, corresponds to a fraction of recrystallized, yet unoriented polymer. This postulation, born out in WAXD observation reported below, is similar to a phenomenon previously reported for compacted polyethylene (PE) fibers [1,2], though with quantitative differences.

Heating the samples above 270 °C effectively destroyed any memory of the compaction history. For the DSC experiments used to collect the data in Fig. 4, the heating scans were run up to 300 °C to ensure that melting of the fibers was complete. A second heating scan, following a controlled cooling at 20 °C/min, yielded the same T_m and crystallinity for all samples (including the original PET fibers) regardless of prior compaction history. That result was not unexpected since the results of the compaction process were destroyed upon heating the sample well above T_m.

In order to understand better the influence of compaction on PET crystallinity and chain orientation, a WAXD study of the materials was pursued. Fig. 5 shows the 2D WAXD patterns of samples prepared at various compaction temperatures, revealing two strong equatorial reflections (normal to the fiber direction) with several symmetric off-equatorial reflections being clearly visible. The equatorial and off-equatorial reflections were consistent with the known triclinic unit cell of PET [30,31]. The primary equatorial reflections retained the sharpness of the original fibers as the compaction temperature increased (Fig. 5(a)–(c)), but broadened when the compaction temperature approached the PET melting point (Fig. 5(d)). The discrete equatorial and off-equatorial reflections eventually disap-

peared when compaction was carried out above the PET melting point, leaving only isotropic rings (Fig. 5(e) and (f)). Above T_m of the PET, the material flowed without constraint, which disrupted the molecular alignment.

The observation of only a minor alteration to the equatorial reflections for compaction temperatures of 255 and 259 °C (see Fig. 5(a)–(c)) was a bit surprising given the significant change in melting behavior and our hypothesis that during compaction the fibers partially melted and recrystallized. We could think of two possible explanations for this result: either (i) primarily lamellar thickening (no melting) occurred at the two lower compaction temperatures, or (ii) melting and recrystallization occurred with geometric confinement of the crystallites, e.g. within the interphase between the oriented fibers, that depended on temperature and affected T_m more than crystallinity. To test (i), preliminary work on compacted PET using SAXS was carried out, but the results (data not shown) clearly indicated that the lamellar thickness (~13 nm) did not change with compaction temperature, prompting us to rule out this mechanism. Explanation (ii) will be discussed later in this paper using mechanical and SEM data.

The degree of crystallinity was calculated from the WAXD patterns in Fig. 5 for comparison with DSC measurements. The degree of crystallinity was calculated from the relative area of the crystalline reflections, Φ_X, by deconvolving the scattering pattern into multiple crystalline peaks and two amorphous peaks using PeakFit™ software and following the procedure described by Wang et al. [30]. The degree of crystallinity calculated from WAXD and DSC experiments are compared in Table 1. The WAXD data yielded slightly higher values, but for compaction temperatures above the PET melting point, the values
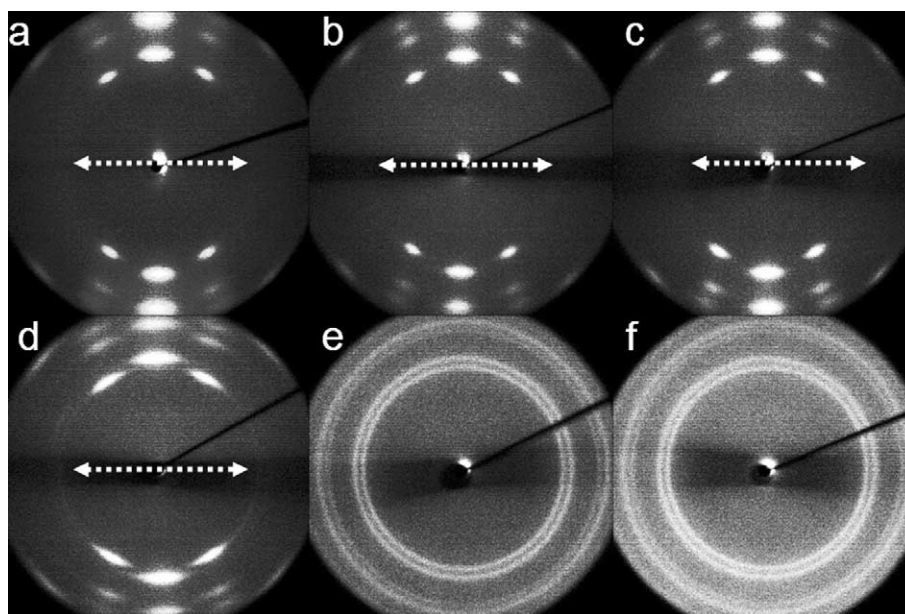

Fig. 5. WAXD patterns of fibers compacted at different temperatures: (a) original PET fibers, (b) 255 °C, (c) 259 °C, (d) 261 °C, (e) 264 °C and (f) 270 °C. Arrows illustrate the direction of the fibers.

obtained from both methods were in good agreement. Additionally, the crystallinity values calculated from WAXD followed the same trend with increasing compaction temperature as the ones calculated from DSC; i.e. the degree of crystallinity was relatively insensitive to compaction temperature. Surprisingly, the crystallinity of the compacted plaques was significantly higher than that of the as-spun PET fibers, see Table 1.

A sharp change in the orientation of the crystalline reflections was observed as the compaction temperature approached the melting temperature, and the molecular orientation was characterized by calculating an orientation parameter using the 010 equatorial reflections from the WAXD patterns. Because the two off-equatorial $0\bar{1}1$ peaks overlap the 010 peak, a correction was made to the raw WAXD data using the PeakFit™ software to fit Gaussian peaks to the 010 peak and the off-equatorial $0\bar{1}1$ satellite peaks and then subtracting the latter from the total intensity curve. The Hermans orientation parameter [32] that quantified the orientation of the 010 plane with respect to the original fiber axis was calculated using Eqs. (3) and (4).

$$f_2 = \frac{3\langle\cos^2\phi\rangle - 1}{2} \tag{3}$$

$$\langle\cos^2\phi\rangle = \frac{\int_{-\pi/2}^{\pi/2} I(\phi)\cos^2\phi \sin\phi \, d\phi}{\int_{-\pi/2}^{\pi/2} I(\phi)\sin\phi \, d\phi} \tag{4}$$

Here, f_2 has limiting values of 1, 0, or $-1/2$ for parallel, random, or perpendicular orientations with respect to the reference direction, respectively. For compaction temperatures between 249 and 255 °C, f_2 was marginally lower than for the original fibers (see Table 1) despite having larger degrees of crystallinity. Some of this reduction may be due to imperfect alignment of the fiber bundles during winding and some to the loss of orientation from partial melting of the fibers during compaction. Nonetheless, in the narrow temperature range $257 < T_{com} < 259$ °C, the measured orientation values are indistinguishable from that of the original fiber for which $f_2 = 0.48$ (FWHM = 11.5°). This preservation of orientation is remarkable, given that the resulting plaques are macroscopically homogenous and have significant transverse mechanical strength (reported below), unlike the original fiber bundles that possess no transverse strength whatsoever. We note that no attempt was made to measure the orientation of the *amorphous* fraction, some 50% of each material, due to the low signal/noise ratio outside of the crystalline peaks. Nevertheless, our observation of a lack of variation in f_2 for most compaction conditions would not necessarily translate to similar invariance in the amorphous phase orientation [33].

As anticipated, the mechanical properties of the PET fiber compactions were anisotropic, and the properties in the longitudinal direction (i.e. the fiber-winding direction) approached those of the original fibers. The flexural moduli in the transverse and longitudinal directions (with respect to the fiber orientation) for plaques compacted at different temperatures are compared in Fig. 6. The modulus of an isotropic plaque, prepared by annealing a compacted plaque at 270 °C and data from Rasburn et al. [3], are also shown in Fig. 6 for comparison. The plaques produced by fiber compaction between 249 and 259 °C had flexural moduli in the longitudinal direction nearly three times higher than that of the isotropic plaques (9.3 GPa vs. 3.4 GPa), while the properties of the compacted material in the transverse direction were lower than for the isotropic material by about 30%. As the compaction temperature increased, the longitudinal flexural modulus of the plaques decreased stepwise near $T_{com} = 255$ °C, with a concomitant increase in the transverse flexural modulus. Rasburn et al. [3] observed similar trends in longitudinal and transverse moduli with compaction temperature, though with quantitative differences attributed to a distinct starting fiber modulus (higher for Rasburn) and different compaction protocol. Importantly, the abrupt change in mechanical properties that we observed was accompanied by an optical transition from clear to translucent appearance, but with no change in either crystalline (010) orientational anisotropy or degree of crystallinity. Thus, it appears that the stepwise change is unrelated to the crystalline fraction of the material, a postulation directly tested later by selective etching of the amorphous fraction for electron microscopy.

The longitudinal and transverse strengths were also examined using flexural testing. As mentioned in the experimental section, testing of transverse specimens led to clear yielding within the 5% strain limit of the ASTM D-790 specification for yield stress; however, longitudinal samples failed less abruptly rendering measurement of the flexural yield stress impossible. To proceed in our comparisons, we considered instead the stress values at the 5% strain limit, here termed '5% flexural strength', as reflective of the flexural strength, noting that at 5% strain the load–displacement curves do show evidence for the onset of yield by downward curvature. Fig. 7 compares the 5% flexural strength values (longitudinal strength) of the compacted materials with the flexural strength of isotropic PET ($T_{com} = 270$ °C); the trends are similar to those for the longitudinal modulus. Specifically, the longitudinal strength of the compacted materials is almost 3 times higher than that of the isotropic with a slight decrease in strength observed with increasing compaction temperature. In comparison, the transverse yield strengths were found to be substantially lower than both the longitudinal strengths and the isotropic yield strength, decreasingly so for increasing compaction temperature. For example at $T_{com} = 249$ °C, the transverse strength was 9.6% that of the longitudinal direction, while at $T_{com} = 259$ °C the value was an improved 16.8%.

It should be noted that the transverse strength of such 'self-reinforced' compacted composites derives primarily from the interfibrillar bonding that apparently improves with increasing compaction temperature at slight expense to longitudinal properties. This is clearly demonstrated in
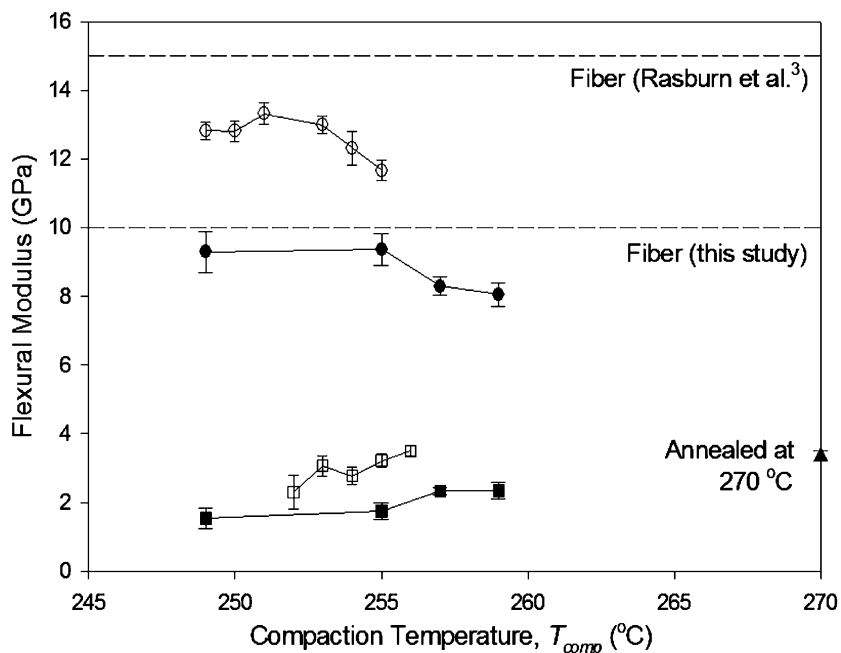
Fig. 6. Plots of flexural moduli as functions of compaction temperature: longitudinal section (●) and transverse section (■). (▲) represents the compacted PET, which was further annealed at 270 °C. Flexural moduli of compactions sectioned longitudinally (○) and transversely (□) previously reported by Rasburn et al. [3] are included for comparison. Note that the modulus of original fiber in Rasburn et al. (15 GPa) is higher than for the present study.

Fig. 7 by the increase of the flexural strength in the transverse direction with increasing compaction temperature. Such apparent increased interfibrillar bonding occurs with little correlation to the degree of crystallinity, measured by either DSC or WAXD, or orientation (Table 1), but with a fairly dramatic up-turn from 255 to 259 °C where we also reported a step-down in longitudinal modulus and an obvious decrease in transparency.

In light of the significant changes in moduli that occurred

without associated changes to the crystalline fraction but with changes to the optical transparency, we sought to elucidate the nature of the amorphous phase distribution in the compacted materials. Thus, the microstructures exhibited by the PET compactions were characterized using electron microscopy and representative results are shown in Fig. 8. In preparing such samples for microscopy, sample cross-sections were etched with n-propylamine, a solvent that selectively removes the amorphous PET in the
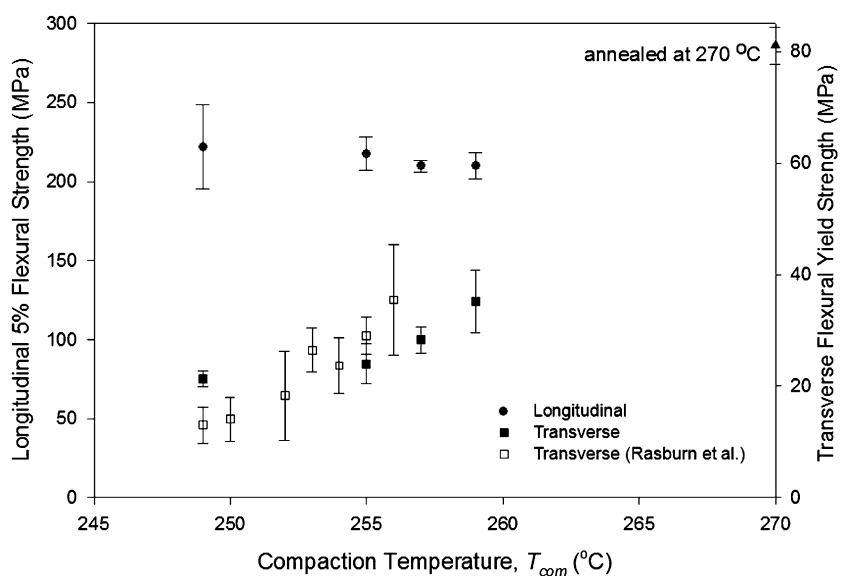

Fig. 7. Plots of longitudinal 5% flexural strength (●) and transverse flexural yield strength (■) as functions of compaction temperature. Note that (▲) represents the flexural strength of compactions further annealed at 270 °C (right scale). (□) represents flexural yield strength in transverse section from the Rasburn et al. [3] study.
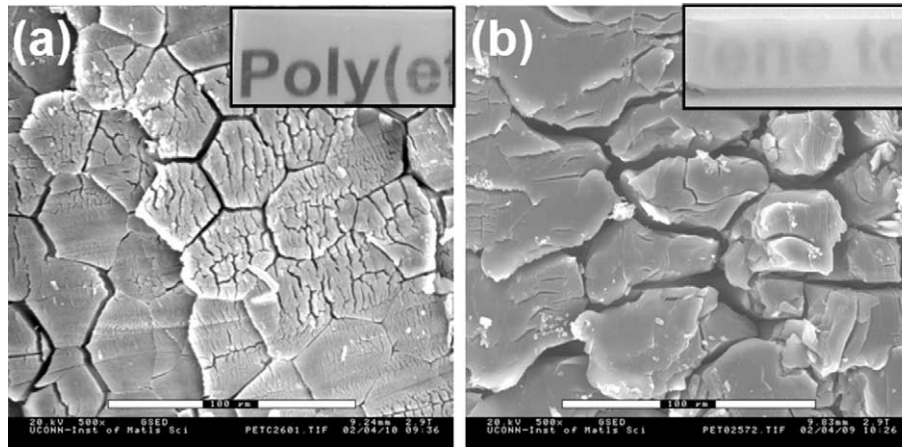
Fig. 8. Electron micrographs of transverse cross-sections from compacted plaques prepared at (a) 255 °C and (b) 259 °C. The scale bar indicates 100 μm. The inset pictures reveal relative transparency levels of the compacted materials.

interfibrillar regions [3]. Fig. 8(a) and (b) shows the plane normal to the fiber orientation for plaques compacted at 255 and 259 °C, respectively. For the sample compacted at $T_{com} = 255$ °C, separate filaments are clearly resolved, though the shape is polygonal, in contrast to the circular shape of the original fibers. That is presumably due to deformation of the fibers at the high temperature and pressure of the compaction process. Moreover, material is clearly etched both from within and between the fibers, indicating that a large fraction of noncrystalline (oriented or disoriented amorphous PET) material exists as fine domains inside the highly crystalline and oriented fibers. For the higher compaction temperature, 259 °C, the shape of the discrete structures is grossly deformed and the average size is considerably greater than the diameter of the original fibers, indicating lateral coalescence. However, some memory of a filamentous structure remained as evidenced by the sharp 'cracks' that resulted from the solvent etching. For this higher compaction temperature, etching removed material almost exclusively from the interfibrillar regions, indicating that the amorphous fraction exists primarily between fibers. This difference in amorphous phase localization between compaction temperatures (at similar degree of crystallinity, Table 1) is manifested in the differences in transparency shown as insets to Fig. 8(a) and (b)). On the basis of these observations, we suggest that the larger longitudinal flexural modulus exhibited for $T_{com} \leq 255$ °C, namely 9.4 GPa vs. 8.1 GPa, is due to a higher orientation of the amorphous phase that is afforded by its fine distribution within the core of compacted fibers. This same suggested amorphous phase orientation contributes to a lower transverse strength (Fig. 7) than that obtained at slightly higher compaction temperatures that localize the amorphous phase to the interfibrillar regions with large domain size and lower uniaxial orientation but a higher component of orientation in the transverse direction.

Having observed the preservation of high internal surface area in the PET compactions and in light of quite ductile

failure in flexural testing of longitudinal compactions, we thought that the materials might feature high impact toughness. Thus, Charpy impact tests were performed on the same samples described above where the compaction temperature, T_{com}, was varied. A representative force–time plot from the impact test of compacted samples is shown in Fig. 9. We observed that the transient impact force increased as the pendulum penetrated through the plaque, then reaching a maximum indicating the onset of cracking and sample failure. The impact force abruptly dropped as the crack propagated, however since the plaques did not break completely (shown below), the impact force shows a prolonged decay to zero. This portion of the force–time trace may be associated with the debonding of fibers as seen visually post-failure in Fig. 10(a). As the compaction temperature increased (data not shown), the force decayed comparatively faster after reaching a maximum, indicating a less ductile fracture and less energy absorption. The plaques produced at temperatures high enough to completely melt the fibers exhibited an abrupt drop in the force after an initial spike, indicating brittle failure. The samples compacted at higher temperature, but still below the PET melting point exhibited a higher peak force and growth time to this force compared to samples prepared at lower compaction temperature. This result is consistent with increased bonding between fibers at the higher compaction temperatures.

Impact toughness of the compacted plaques was calculated from the cumulative energy absorbed during the impact test using Eq. (2), and this quantity is plotted as a function of compaction temperature in Fig. 11. We see that the impact toughness decreased slightly with increasing compaction temperature from 249 to 257 °C and then decreased more significantly for the 259 °C preparation. The isotropic plaque, prepared at 270 °C was considerably more brittle, exhibiting an impact toughness only about 10% that of the compacted plaques. This observed trend in impact toughness is supported qualitatively by visual observations
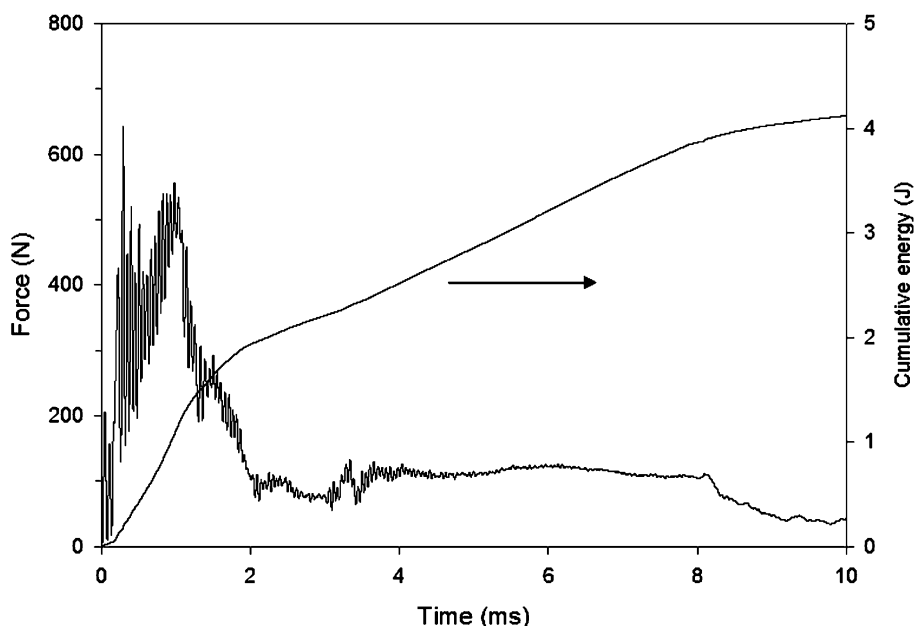
Fig. 9. Representative results of Charpy impact testing showing plots of impact force and cumulative energy as a functions of time for $T_{com} = 249\,^{\circ}C$.

of the failed specimens. Fig. 10 shows photographs of the damaged samples after impact testing. Fracture was attended by extensive splitting along the fiber direction and complete separation along the edge under impact load (Fig. 10(a) and (b)), the arrows indicating the direction and location of impact. A large number of isolated fibers, or small fiber bundles, was exposed by fracture for $T_{com} =$

249 °C (Fig. 10(a)), while larger fiber bundles were exposed by fracture of materials prepared at higher compaction temperatures (Fig. 10(b) and (c)). These results are consistent with stronger interfibrillar bonding, but lower impact toughness for the plaques compacted at higher temperatures. Samples compacted at 270 °C failed in a completely different manner (Fig. 10(d)), shattering into multiple, irregularly shaped pieces, indicating brittle failure, which is consistent with the relatively low impact strength shown in Fig. 11.
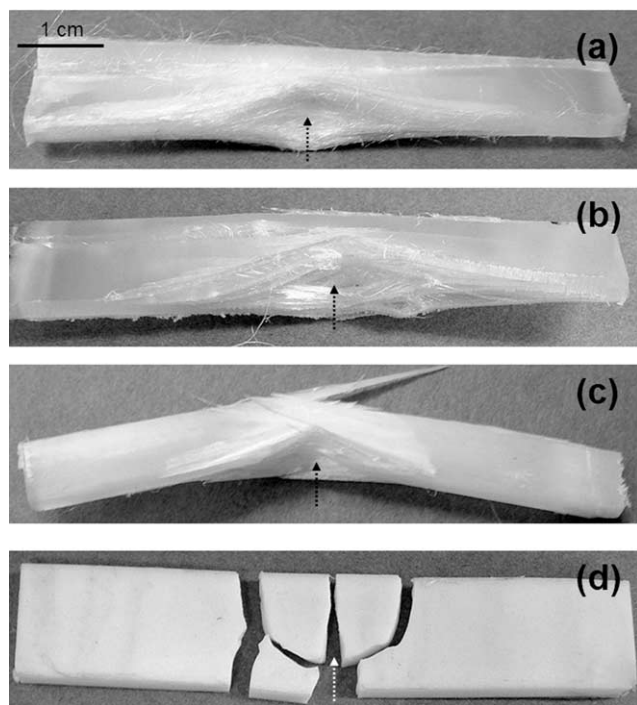
4. Conclusions

A simplified process involving one pressure step and one temperature step was developed for hot compaction of PET fibers. The compaction temperature was the key variable in the production of quality compacted plaques; varying the compaction pressure between 20 and 60 MPa having a relatively small influence on the properties of the plaques produced. Plaques produced by compaction at $T_{com} = 255\,^{\circ}C$ and lower were relatively clear, high in flexural modulus, and weak in transverse strength. Increasing the compaction temperature above 255 °C reduced the clarity of the plaque, presumably due to increased scattering from the melted and recrystallized regions between the original fibers, while increasing the transverse mechanical properties.

Attempts were made to understand the trends in compaction mechanical properties in terms of the PET crystallinity and orientation of the crystalline fraction. Using DSC and WAXD analyses, we found that compaction with increasing temperature had a significant effect on the

Fig. 10. Photographs of impact tested specimens: (a) compacted at 249 °C, (b) compacted at 257 °C, (c) compacted at 259 °C and (d) annealed at 270 °C. Arrows illustrate the direction and location of the pendulum impact.
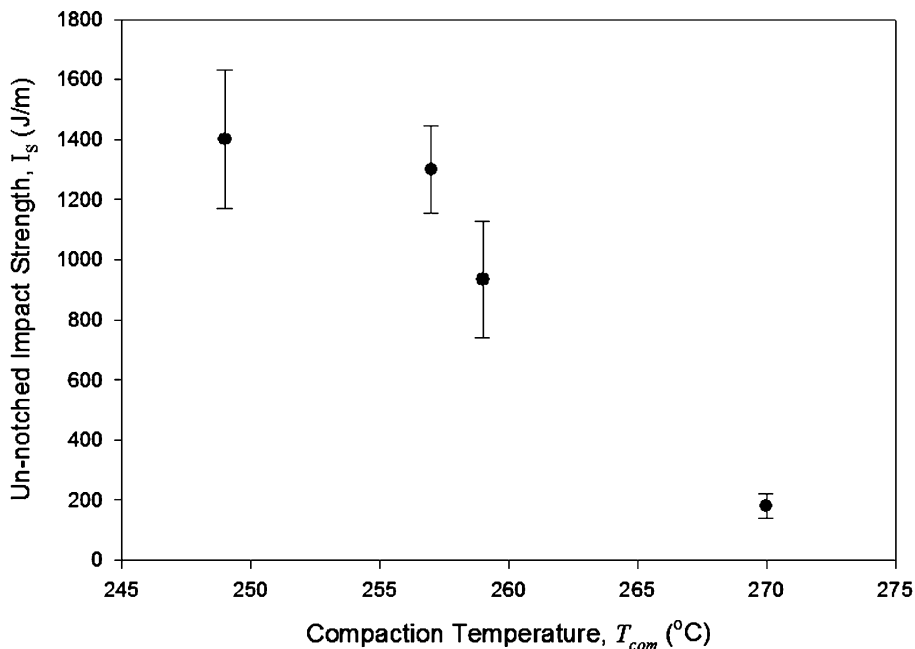
Fig. 11. Comparison of un-notched Charpy impact strength of PET fiber sheets between after compaction (at the temperature of 249, 257 and 259 °C) and isotropic (i.e. annealed at 270 °C).

melting temperature, similar qualitatively to that observed for annealing at ambient pressure, but had little effect on the degree of crystallinity. Measurements of the Hermans orientation parameter, f_2, showed little differences among samples, except that as compaction temperature approached the melting point of the original fibers (262 °C), the orientation decreased. For compaction temperatures above 262 °C, the plaques became nearly isotropic.

Because of the retention of the fiber orientation in the compacted plaques, their properties were highly anisotropic. The flexural modulus for samples cut in the fiber direction was within 10% of that of the original fibers for compactions done below 255 °C and within 20% for compactions done at greater than 255 °C, but below the melting point of the fibers. The modulus in the direction transverse to the fiber orientation was much lower, but increased a little with increasing compaction temperature. For a plaque compacted at 259 °C, the transverse flexural modulus was about 30% less than that of an isotropic plaque, while the longitudinal modulus was more than twice the modulus of the isotropic plaque. Similarly, the flexural yield strength was much greater for samples cut in the longitudinal direction than in the transverse direction, the latter being lower than that of an isotropic plaque. The difference between the longitudinal and transverse yield strengths decreased with increasing compaction temperature. The transverse strength increase was due to enhanced interfibrillar adhesion between fibers as a result of the melting and recrystallization of the fiber surfaces.

Compaction greatly enhanced the impact toughness of the PET plaques. An isotropic plaque exhibited brittle fracture in an unnotched impact test, while the compacted materials were ductile in failure and had impact strengths 5–7 times higher than that of an isotropic plaque, which is a consequence of the retention of the fiber orientation and the large interfacial region between fibers that provides a convenient mechanism for energy absorption. As a result, such materials may have applicability for protective coatings or films or in other applications requiring high impact energy absorption.

Acknowledgements

References

[1] Hine PJ, Ward IM, Olley RH, Bassett DC. J Mater Sci 1993;28: 316–24.
[2] Kabell MA, Bassett DC, Olley RH, Hine PJ, Ward IM. J Mater Sci 1994;29:4694–9.
[3] Rasburn J, Hine PJ, Ward IM, Olley RH, Bassett DC, Kabeel MA. J Mater Sci 1995;30:615–22.
[4] El-Maaty MIA, Bassett DC, Olley RH, Hine PJ, Ward IM. J Mater Sci 1996;31:1157–63.
[5] Hine PJ, Ward IM. J Mater Sci 1996;31:371–9.
[6] Oiley RH, Bassett DC, Hine PJ, Ward IM. J Mater Sci 1993;28: 316–24.
[7] Yan RJ, Hine PJ, Ward IM, Oiley RH, Bassett DC. J Mater Sci 1997; 32:4821–32.

[8] Hine PJ, Ward IM, Jordan ND, Oiley RH, Bassett DC. J Macromol Sci Phys 2001;B40:959–89.

[9] Jordan ND, Oiley RH, Bassett DC, Hine PJ, Ward IM. Polymer 2002; 43:3397–404.

[10] Hine PJ, Bonner M, Brew B, Ward IM. Plast Rubber Compos Process Appl 1998;27:167–71.

[11] Hine PJ, Ward IM, Jordan ND, Oiley RH, Bassett DC. Polymer 2003; 44:1117–31.

[12] Jordan ND, Bassett DC, Oiley RH, Hine PJ, Ward IM. Polymer 2003; 44:1133–43.

[13] Hine PJ, Ward IM. J Appl Polym Sci 2004;91:2223–33.

[14] Hine PJ, Ward IM. Polymer 2004;45:1423–37.

[15] Ward IM, Hine PJ. Polym Eng Sci 1997;37:1809–14.

[16] Cohen Y, Rein DM, Vaykhansky L. Compos Sci Technol 1997;57: 1149–54.

[17] Rein DM, Shavit L, Khalfin RL, Cohen Y, Terry A, Rastogi S. J Polym Sci, Polym Phys 2004;42:53–9.

[18] Rein DM, Vaykhansky L, Khalfin RL, Cohen Y. Polym Adv Technol 2002;1046–54.

[19] Stellbrink KKU, Hausser G, Steegmuller R. J Thermoplast Compos Mater 1999;12:188–200.

[20] Wright DD, Gilbert JL, Lautenschlager EP. J Mater Sci: Mater Med 1999;10:503–12.

[21] Wright DD, Lautenschlager EP, Gilbert JL. J Biomed Mater Res 1998;43:153–61.

[22] Xu T, Farris RJ. Proceedings of the 61st Annual Technical Conference and Exhibition. XLIX.: Society of Plastics Engineers; 2003 p. 2156–60.

[23] Blundell DJ, MacKerron DH, Fuller W, Mahendrasingam A, Martin C, Oldman RJ, Rule RJ, Riekel C. Polymer 1996;37:3303–11.

[24] Mahendrasingam A, Martin C, Fuller W, Blundell DJ, Oldman RJ, Harvie JL, MacKerron DH, Riekel C, Engstrom P. Polymer 1999;40: 5553–65.

[25] Blundell DJ, Mahendrasingam A, Martin C, Fuller W, MacKerron DH, Harvie JL, Oldman RJ, Riekel C. Polymer 2000; 41:7793–802.

[26] Meyerhoff G, Shimotsuma S. Makromol Chem 1970;135:195–217.

[27] Blundell DJ, Osborn BN. Polymer 1983;24:953–8.

[28] Chu C-M, Wilkes GL. J Macromol Sci Phys 1974;B10:551–78.

[29] Miyagi A, Wunderlich B. J Polym Sci, Part A-2 1972;10:1404–5.

[30] Wang ZG, Hsiao BS, Fu BX, Liu L, Yeh F, Sauer BB, Chang H, Schultz JM. Polymer 1999;41:1791–7.

[31] Tomashpol'skii YY, Markova GS. Vysokomol Soyed 1964;6:274–80.

[32] Roe R-J. Methods of X-ray and neutron scattering in polymer science. New York: Oxford University Press; 2000.

[33] Fu YG, Annis B, Boller A, Jin YM, Wunderlich B. J Polym Sci Part B—Polym Phys 1994;32:2289–306.